공학석사 학위논문

Ca-La M-type 육방정 페라이트 합성과 자기적 특성

Synthesis and Magnetic Properties of Ca-La M-type Hexaferrite

2017 년 2 월

서울대학교 대학원

재료공학부

얀 웨 이

Abstract

Ca-La M-type hexaferrites have been reported to exhibit high saturation magnetization (M_s) and coercivity (H_c) comparable to those of Sr or Ba M-type hexaferrites. In this study, we tried to synthesize the single phase of $Ca_{0.5}La_{0.5}Fe_{12-y}O_{19-\delta}$ and investigated the effects of iron deficiency on structural and magnetic properties in $Ca_{0.5}La_{0.5}Fe_{12-y}O_{19-\delta}$ ($0.75 \leqq y \leqq 2.15$) M-type hexaferrites.

Ca-La M-type hexaferrite powder samples having the nominal compositions of $Ca_{1-x}La_xFe_{12}O_{19}$ (x=0.4, 0.5 and 0.6) and $Ca_{0.5}La_{0.5}Fe_{12-y}O_{19-\delta}$ ($0.75 \leqq \boldsymbol{y} \leqq 2.15$) were prepared by conventional solid state reaction. All the precursor powders used (La_2O_3, $CaCO_3$, and Fe_2O_3) in this study were 99.9% purity. Precursor powders were weighed, ball-milled for 24 h, and then uniaxially pressed into pellets. As-pressed pellets were calcined at 1150, 1200, 1250, and 1300 ℃ for 12 h in air, to check whether the single phase of M-type hexaferrite can be formed or not. The calcination was repeated twice by intermediate ball milling and pelletizing. As-calcined powders were pressed into pellets uniaxially. To measure the magnetic properties of samples, the pellets were put into a muffle furnace and sintered at 1275, 1300 and 1325℃ for 4 h in air. Phases and lattice parameters of sintered samples were analyzed

by powder X-ray diffraction (XRD). Microstructure was observed by Field Emission-scanning electron microscopy (FE-SEM) and magnetic properties were measured by Vibrating Sample Magnetometer (VSM).

XRD patterns showed all the phases in the $Ca_{0.5}La_{0.5}Fe_{12-y}O_{19-\delta}$ ($1.75 \leqq \mathbf{y} \leqq 2.15$) calcined at 1250 for 12 h and $Ca_{0.5}La_{0.5}Fe_{12-y}O_{19-\delta}$ ($0.75 \leqq \mathbf{y} \leqq 2.15$) calcined at 1300℃ for 12 h were the single phases with hexagonal structure. For the single phases of $Ca_{0.5}La_{0.5}Fe_{12-y}O_{19-\delta}$, at a given sintering temperature, the lattice parameter *a*, *c* and unite cell volume of the $Ca_{0.5}La_{0.5}Fe_{12-y}O_{19-\delta}$ single phases were all firstly decreased and increased later with increasing ***y,*** at a given sintering temperature. The average grain sizes are firstly increased and then decreased with increasing ***y***. The saturation magnetization M_s decreased insignificantly with increasing ***y***. The highest M_s value of 77.5 emu/g was obtained from the $Ca_{0.5}La_{0.5}Fe_{12-y}O_{19-\delta}$ ($y = 0.75$) sample sintered at 1300℃ for 4 h in air, which is higher than those of pure phase SrM and BaM by 11.2% and 14.5%, respectively. As ***y*** is increased, H_c first was decreased and then increased for both systems.

In conclusion, iron deficiency could facilitate the formation of single phase Ca-La M-type hexaferrite. The compound $Ca_{0.5}La_{0.5}Fe_{12-y}O_{19-\delta}$ was calcined for 12 h in air at 1250 and 1300℃, and their Fe solubility limits were $1.75 \leqq \boldsymbol{y} \leqq 2.15$ and $0.75 \leqq \boldsymbol{y} \leqq 2.15$ respectively. Iron deficiency could Iron deficiency

could improve the magnetic properties of Ca-La M-type hexaferrites.

Key Words: magnetoplumbite, iron-deficiency, hexaferrite, Ca-La M-type hexaferrite, solid state reaction, saturation magnetization, coercivity.

Student ID: 2014-25146

Contents

1. Introduction

Hexagonal ferrites have been widely applied as the permanent magnet, microwave, magneto-optical, and high-density magnetic recording media due to their excellent oxidation resistance, higher coercivity, remanence, magnetic energy product, and uniaxial magnetocrystalline anisotropy [1-4].

The crystal structure of SrM is comprised by alternative stacks of spinel (S, Fe_6O_8) and hexagonal (R, $SrFe_6O_{11}$) blocks in the form of RSR*S*, where* denotes 180° rotation around the hexagonal c-axis [5]. In the unit cell, 24 Fe^{3+} ions occupy five different crystallographic sites of oxygen lattice, one tetrahedral ($4f_1$), three octahedral (12k, 2a, $4f_2$), and one hexahedral (2b) sites. The spins of Fe^{3+} ions in these sites are ferromagnetically coupled through super exchange interaction with the oxygen ions causing the spins in 2a, 12k, and 2b sites to align parallel to the crystallographic c axis and those in $4f_1$ and $4f_2$ sites to align anti-parallel. The net magnetic moment from a molecular formula of $SrFe_{12}O_{19}$ occupying half of the unit cell is 20 μ_B.

Recently, the focus on obtaining high performance hexagonal ferrites has driven the research to a wide range of areas. On the one hand, the adjustment of microstructure, preparation of single domain particles and increased sintering density [5] was found to improve coercivity and remanence

while the other aspect was substitution or combine substitution to achieve ion substitution, thereby increasing the saturation magnetization and corevicity [6-10]. Nowadays method such as rare earth ions substitution for improving the magnetic properties, study of exchange interaction and the magnetocrystalline anisotropy mechanisms have become popular in this field [11-14].

The composition of magnetoplumbite M-type ferrites is usually characterized by the chemical formula $MFe_{12}O_{19}$ where M stands for Ba, Sr, or Pb [15]. According to the accepted phase diagram of the CaO-Fe_2O_3 system [16], pure $CaO{\cdot}6Fe_2O_3$ with a magnetoplumbite (M) structure does not exist. However, in 1963, Ichinose et al. [17] reported that the M-type calcium ferrite could be formed by adding a small amount of La_2O_3. Although Yamamoto et al. [18-20] studied this La^{3+}-doped calcium ferrite extensively and in 1992, Fang et al. [15] studied $Ca_{1-x}La_xFe_{12}O_{19}$ system, and the studies on hexagonal ferrite were restricted to formation mechanisms, defect structure and crystal structure and other features remain unexplored.

In this experiment, samples were prepared by solid state reaction based on lower Fe^{3+}/Ca^{2+} and La^{3+} enhancing the ionic diffusion and improving the magnetic properties through decreasing the content of Fe ion. In the present study, we investigated single phase synthesis condition, the effect of iron

deficiency and sintering temperature has on crystal structure and microstructure and magnetic properties.

2. Background

2.1 Crystal structure of M type hexaferrites

M-type ferrite, $BaFe_{12}O_{19}$, has lattice constants a= 5.89A˚ and c= 23.19 A˚ in a hexagonal closed packed lattice of oxygen and Ba with Fe in octahedral (12k, $4f_2$, and 2a), tetrahedral ($4f_1$), and hexahedral (2b) sites. The Fe ions are the sole source of magnetic moment: the 12k, 2a, and 2b sites are spin up and $4f_1$ and $4f_2$ sites are spin down, as indicated in Fig.2-1. The general structure of M type hexaferrite ($AO{\cdot}6Fe_2O_3$ or $AFe_{12}O_{19}$, where A is a divalent ion such as Ba^{2+} ,Sr^{2+}, Pb^{2+}, etc.), which is hexagonal with space group P63/mmc, is constructed from 4 building blocks, namely S, S*, R, and R* in Fig.1-2. The oxygen atoms are closed packed with the A and Fe ions in the interstitial sites. There are ten layers of oxygen atoms along the c axis and the iron atoms are positioned at five different sites. The S (Fe_6O_8) and S* blocks are spinels with two oxygen layers and six Fe^{3+} ions. Four of these Fe^{3+}ions are in the octahedral sites with their spins aligned parallel to each other. The remaining two Fe^{3+} ions are in tetrahedral sites and have their spins antiparallel to those that are at the octahedral sites. As shown in Fig. 2-2 the hexagonal R (AFe_6O_{11}) and R* blocks consist of three oxygen layers with one of the oxygen anions replaced with an A ion (A= Ba / Sr / Pb). Each R block contains six Fe^{3+} ions, of which five are in octahedral sites, three having spin up and two having spin

down.

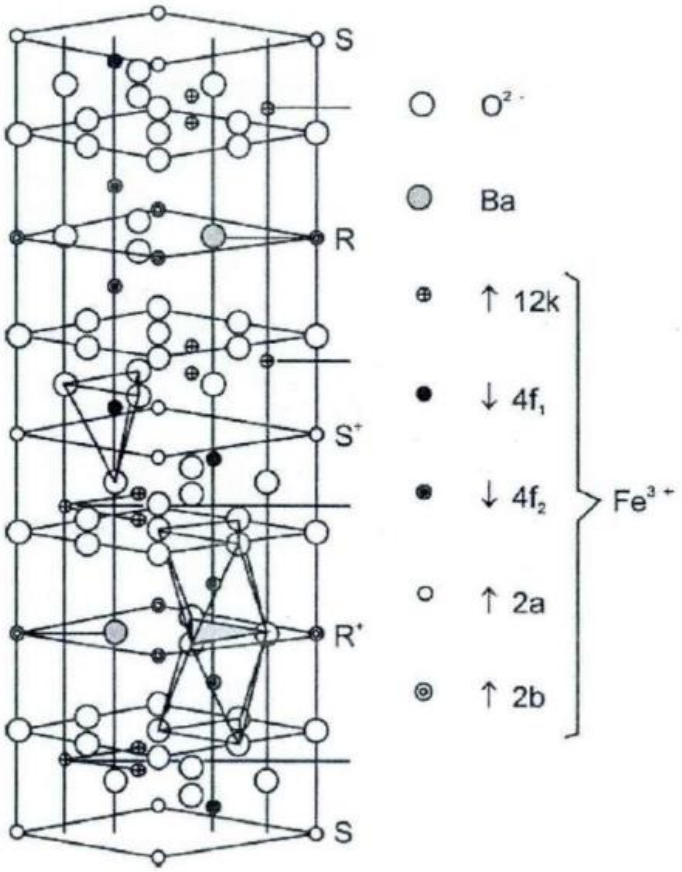

Figure 2-1 Crystal structure of M-type hexaferrites [22]

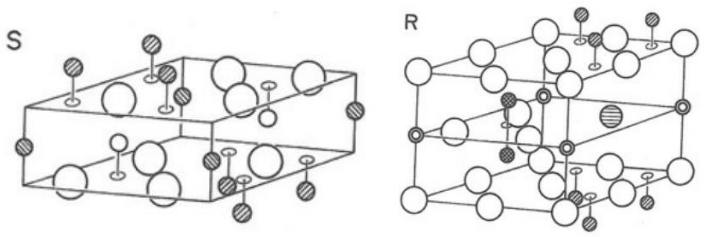

Figure 2-2 Perspective drawing of S block (left) and R block (right) [22].

2.2 Magnetic properties of M type hexagonal ferrite

2.2.1 Saturation magnetization M_s and Remanence M_r

When a magnetic field is imposed on the material, domains that are nearly lined up with the field grow at the expense of unaligned domains. As the field increases in strength, favorably oriented domains grow more easily, unfavorably oriented domains disappear and rotation completes the alignment of the domains with the field. The saturation magnetization($\boldsymbol{M_s}$), produced when all of the domains are oriented along with the magnetic field, is the greatest amount of magnetization that the material can obtain.

When the applied field reduced to zero after magnetizing a magnetic material the remaining magnetization is called the remanence (M_r).

M type hexaferrite unit cell consists of RSR * S* block, contains two $BaFe_{12}O_{19}$ molecule, so the molecular magnetic moment from a molecular of $BaFe_{12}O_{19}$ occupying half of the unit cell and Fe^{3+} ion magnetic moment of $5\mu_B$, thus the $BaFe_{12}O_{19}$ theoretical values of the molecular magnetic moments are as follows (2-1) [24]:

$$(n_B)_M = 5[(4-2)+(3-2+1)] = 5(7+1-2-2) = 20\mu_B \qquad (2\text{-}1)$$

The results coincide with the theoretical result [25].

2.2.2 Coercivity H_c

The induced magnetization can be reduced to zero by applying a reverse field of strength H_c. It is a microstructure-sensitive property which mainly depends on magnetocrystalline anisotropy and grain size.

2.2.3 Magnetocrystalline anisotropy

The magnetocrystalline anisotropy represents the degree to which the magnetic material is magnetized in different directions, and thus it is an important parameter of hexagonal ferrite, the expression as shown in equation (2-2) [26]:

$$E_K = K_0 + K_1 \sin^2\theta + K_2 \sin^4\theta + K_3 \sin^6\theta \bullet \cos 6\phi \qquad (2\text{-}2)$$

Where$\theta$is the angle between the direction of magnetisation and c-axis, K_0 is the energy to magnetise the easy axis. ϕ is the azimuth angle of M_s projected in the plane perpendicular to the hexagonal axis [0001], we generally only consider the terms associated with θ, K. For the hexagonal ferrite of three magnetocrystalline anisotropy constants, in general, the equation (2-2) is only accurate to the quadratic term of sinθ, the equation (2-2) can be simplified as (2-3) [26]:

$$E_K = K_0 + K_1 \sin^2\theta + K_2 \sin^4\theta \qquad (2\text{-}3)$$

Because the difference of between K_1 and K_2 and sizes, the anisotropy of the magnet can occur in three easy magnetization direction: (1) easy axis - hexagonal axis [0001]; (2) easily magnetized plane - perpendicular to the [0001] axis; and (3) a conical plane with an angle to [0001].

2.3 Cation substitution of M type hexaferrites

2.3.1 Me substitution in M type hexaferrites

Me Ions substitution from $MeFe_{12}O_{19}$ is the most common method of substitution, which approaches more stable crystal structure to enhance the magnetic anisotropy and thus obtain more excellent magnetic properties. Ion radius similar principle is commonly used in ion substitution. Many studies investigated that the substitution of rare earth ions improving the performance of ferrite materials [27].

2.3.2 Fe ion substitution in M type hexaferrites

Fe ions have 2a, $4f_2$, and 12 k, $4f_1$ and 2b five different crystal positions, in the five crystal positions. At $4f_1$, $4f_2$ the direction of magnetic moments is spin down. Therefore, some non-magnetic properties can substitute the magnetic iron ions at the $4f_1$, $4f_2$ position. Substitution can weaken the

opposite direction of the magnetic moment to a certain degree to get more Bohr magnetic number and thus, to increase saturation magnetization [28].

2.3.3 Ion co-substitution in M type hexaferrites

In recent studies, the study on ion co-substitution is much more focused upon instead of separate substitution of Me ion or Fe ion in the past.

The most common ion-coordinated substituents reported in the literature are La^{3+}-Co^{2+} substitutions which lead to significant enhancement in the H_c without reducing the M_s [29]. Co^{2+}-Ti^{4+} co-substituted Fe^{3+} induced decrease of the coercivity without change of saturation magnetization [30]. Zn^{2+}-Nb^{4+}co-substituted Fe^{3+} resulted in 30 % enhancement of saturation magnetization and 34% decline of the coercivity [31]. Zn^{2+}-Ti^{4+}co-substituted Fe^{3+} lead to a decline of saturation magnetization and coercivity [32]. La^{3+}-Zn^{2+}substituted Sr^{2+}-Fe^{2+} induce 4% increase of saturation magnetization with no change of magnetocrystalline anisotropy field [33].

3. Experimental

3.1 Synthesis of Ca-La hexaferrites

Ca-La M-type hexaferrite (CaLaM) powder having the nominal compositons of $Ca_xLa_{1-x}Fe_{12}O_{19}$ (***x***=0.4, 0.5, 0.6) and $Ca_{0.5}La_{0.5}Fe_{12-y}O_{19-\delta}$ (***y***=1.75, 2, 2.25) were prepared by conventional solid state reaction. In this study, all the precursor powders were used (La_2O_3, $CaCO_3$, Fe_2O_3) 99.9% purity. Precursor powders were prepared by weighting and ball-milling for 24h in a plastic container with zirconia balls and 99.99% ethanol. The solution was dried in over at 60℃, grounded, and sieved to 100 mesh. Precursor Powders were uniaxially pressed for pellet within inside 2 inch mold. Green body pellets were calcined at 1150, 1200, 1250, 1300℃ for 12 h in air. The calcination was repeated twice by intermediate ball milling and pelletizing. Double calcinations were performed for the complete solid state reaction and compositional homogeneity of the samples. As-calcined powders were pressed for pellets uniaxially, the pellets were sintered at 1275, 1300, 1325℃, for 4 h in air.

3.2 Characterization

3.2.1 X-ray diffractometer (XRD) analysis of crystallinity and phase of $Ca_xLa_{1-x}Fe_{12}O_{19}$ ($0.4 \leqq x \leqq 0.6$) and $Ca_{0.5}La_{0.5}Fe_{12-y}O_{19-\delta}$ ($1.75 \leqq y \leqq 2.25$)

$Ca_xLa_{1-x}Fe_{12}O_{19}$($0.4 \leqq x \leqq 0.6$) and $Ca_{0.5}La_{0.5}Fe_{12-y}O_{19-\delta}$ ($1.75 \leqq y \leqq 2.25$) were analyzed by X-ray diffractometer (Bruker Miller Co.D8-advance). XRD was measured by using Cu Kα1 with 1.54056 wave length, voltage and current were 40 kV and 40 mA.

3.2.2 Microstructure observation using field emission scanning electron microscopy (FE-SEM)

FE-SEM (JEQL, JSM-6330F) was used to observe the microstructure of sample. Polishing and chemical etching were required for better observation of microstructure. The etching condition of the sample was treated with 35% HCL at 90 to 105 ℃ for 20 seconds.

3.2.3 Measurement of magnetic properties

Magnetic properties were measured at room temperature with vibrating sample magnetometer (VSM-7410). The maximum applied field of 25kOe was used to evaluate the magnetic parameters.

3.2.4 Measurement of sintered density

The sintered density is measured using the Archimedes method. First, the sintered samples were immersed in distilled water and heated for 1 h. After removing distilled water in pore the surface, the weight W_{sat} and W_{fluid} were weighted, respectively. Then dry the samples for 2 h and the weight of W_{air} was measured. The experimental density (ρ_1), theoretical density (ρ_2) and relative density ($\rho_{\%}$) was calculated by the equation (3-1), (3-2) and (3-3) as follows:

$$\rho_1 = \frac{W_{air}}{(W_{sat} - W_{fluid})} \qquad (3\text{-}1)$$

$$\rho_2 = \frac{2M}{NV_{cell}} \qquad (3\text{-}2)$$

$$\rho_{\%} = \frac{\rho_1}{\rho_2} \qquad (3\text{-}3)$$

(M: molecular weight, N: Avogadro constant, V_{cell}: unite cell volume)

4. Result and Discussion

4.1 Crystal structure of $Ca_xLa_{1-x}Fe_{12}O_{19}$ ($0.4 \leqq x \leqq 0.6$)

Figure 4-1, 4-2 and 4-3 showed X-ray diffraction (XRD) patterns of the calcined powders of $Ca_{1-x}La_xFe_{12}O_{19}$ ($0.4 \leqq x \leqq 0.6$) with varying temperature from 1150 to 1300℃ for 12 h in air. The XRD patterns of x=0.6 at calcination 1300℃(Figure 4-3) showed single phase M-type hexagonal structure. The results were listed in Table 4-1.

The XRD patterns of $Ca_{1-x}La_xFe_{11}O_{19-\delta}$ ($0.4 \leqq x \leqq 0.6$) calcined powder at 1150 - 1300 ℃ for 12 h to study the effects of iron deficiency was shown in Figures 4-4 and 4-7. The results were listed in Table 4-2.

Comparing the results listed in Table4-2, 4-3, it was found that it could facilitate the formation of a single phase of $Ca_{1-x}La_xFe_{11}O_{19-\delta}$ ($0.4 \leqq x \leqq 0.6$) according to the decrease in iron content.

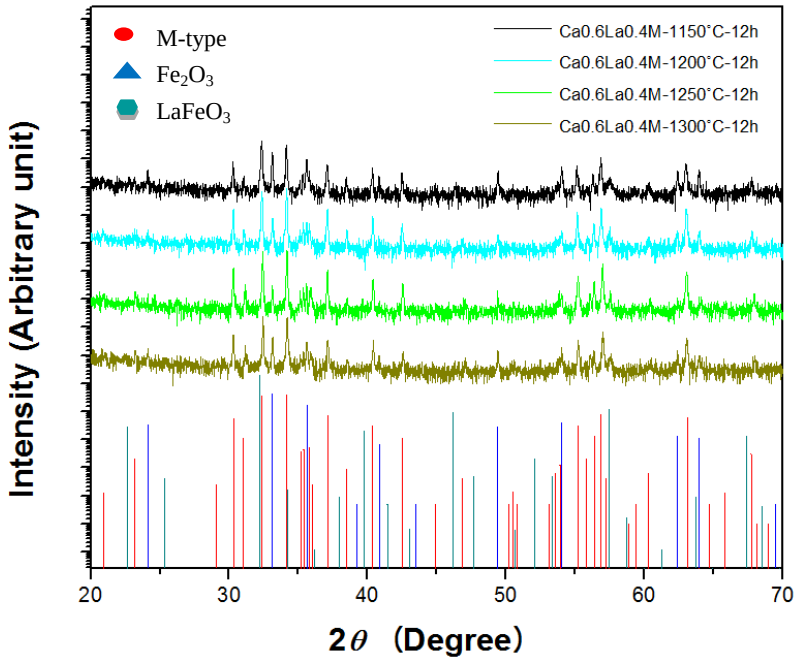

Figure 4-1 XRD patterns of $Ca_{0.6}La_{0.4}Fe_{12}O_{19}$ calcined in air

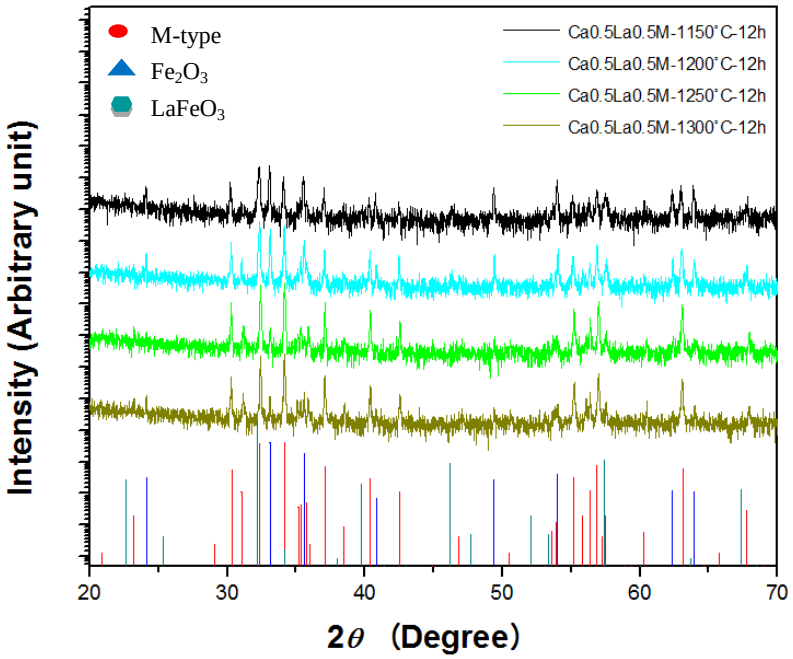

Figure 4-2 XRD patterns of $Ca_{0.5}La_{0.5}Fe_{12}O_{19}$ calcined in air

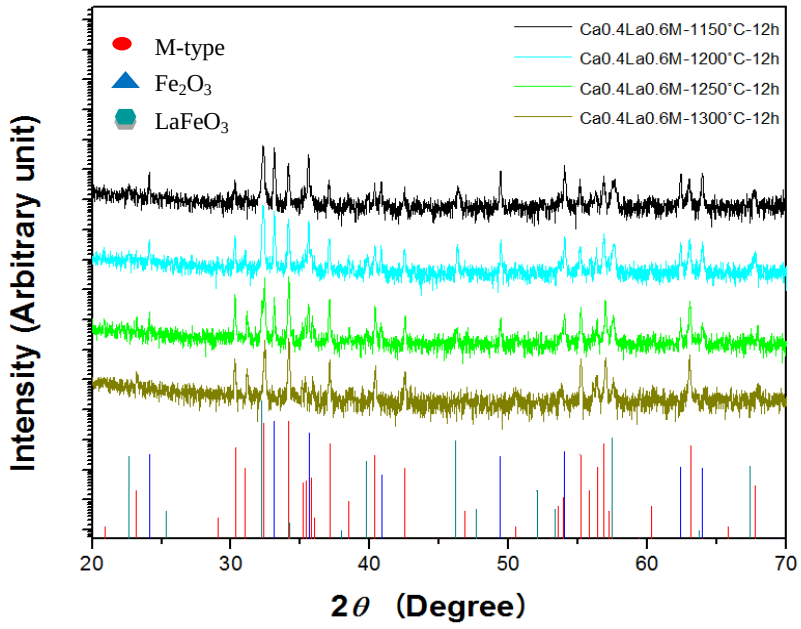

Figure 4-3 XRD patterns of $Ca_{0.4}La_{0.6}Fe_{12}O_{19}$ calcined in air.

Table 4-1 Detected phases from XRD patterns of $Ca_{1-x}La_xFe_{12}O_{19}$ after calcination in air

Temperature (℃) / Composition.x	1150	1200	1250	1300
x=0.4	M+h	M+h	M+h	M+h
x=0.5	M+h+L	M+h+L	M+h	M+h
x=0.6	M+h+L	M+h+L	M+h+L	M

M: M-type phase h: hematite L:$LaFeO_3$

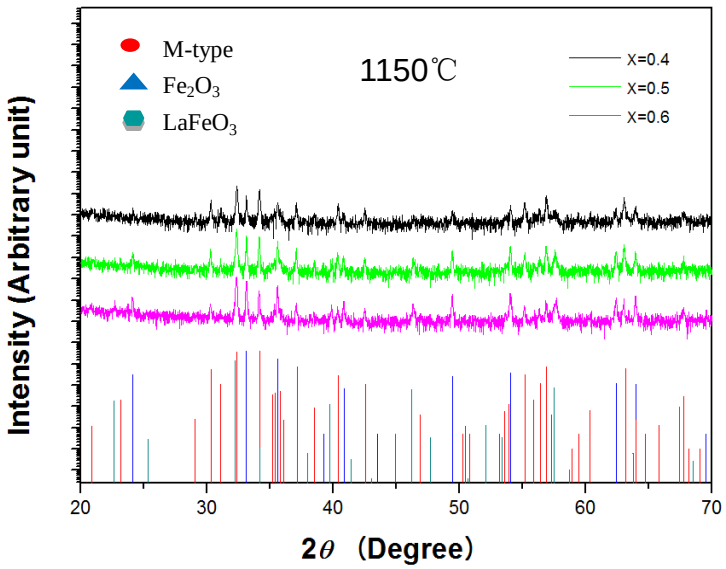

Figure 4-4 XRD patterns of $Ca_{1-x}La_xFe_{11}O_{19-\delta}$ calcined in air.

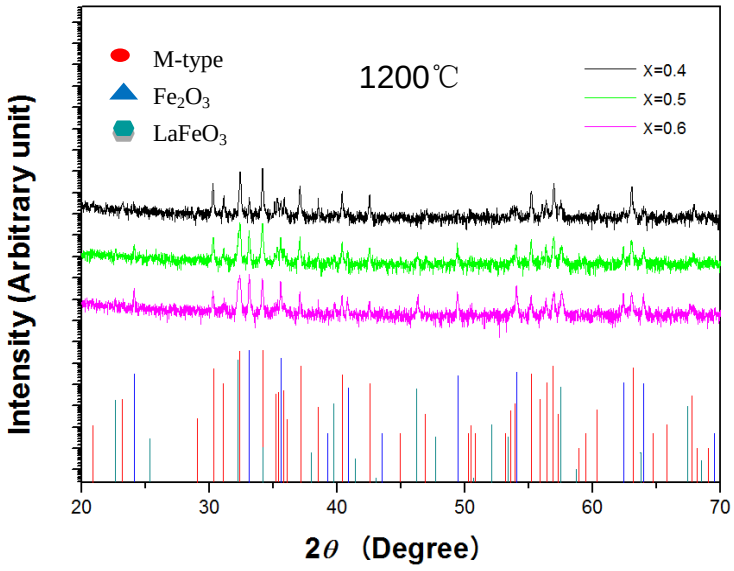

Figure 4-5 XRD patterns of $Ca_{1-x}La_xFe_{11}O_{19-\delta}$ calcined in air.

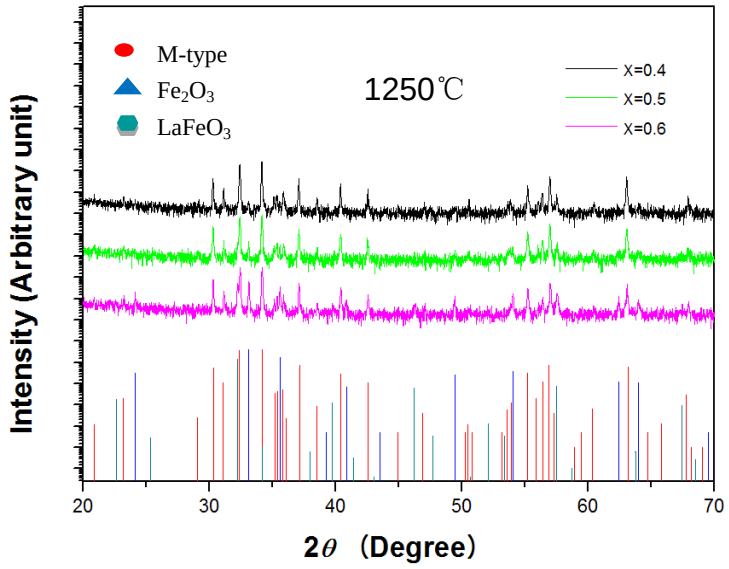

Figure 4-6 XRD patterns of $Ca_{1-x}La_xFe_{11}O_{19-\delta}$ calcined in air

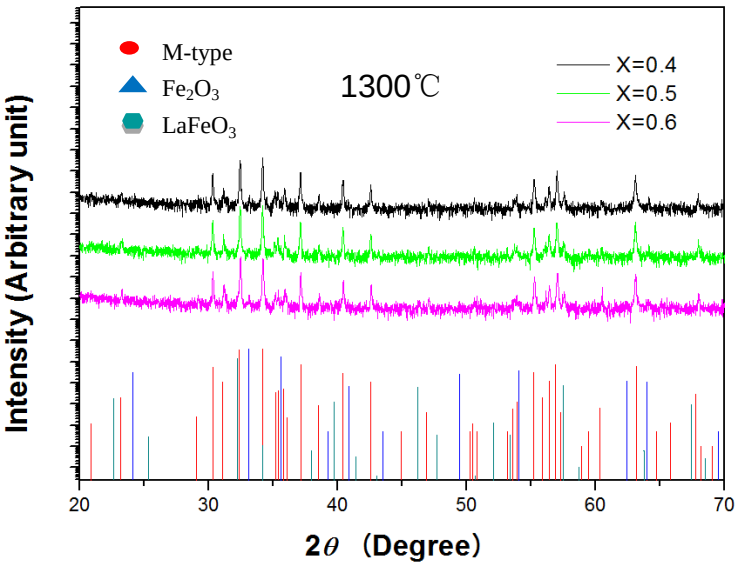

Figure 4-7 XRD patterns of $Ca_{1-x}La_xFe_{11}O_{19-\delta}$ calcined in air

Table 4-2 Detected phases from XRD patterns of $Ca_{1-x}La_xFe_{12}O_{19}$ after calcination in air

Temperature (℃) / Composition.x	1150	1200	1250	1300
x=0.4	M+h	M+h	M+h	M+h
x=0.5	M+h+L	M+h+L	M+h	M+h
x=0.6	M+h+L	M+h+L	M+h+L	M

Table 4-3 Detected phases from XRD patterns of $Ca_{1-x}La_xFe_{11}O_{19-\delta}$ after calcination in air

Temperature (℃) / Composition.x	1150	1200	1250	1300
x=0.4	M+h	M+h	M	M
x=0.5	M+h+L	M+h+L	M+h	M
x=0.6	M+h+L	M+h+L	M+h+L	M+L

M: M-type phase h: hematite L:$LaFeO_3$

4.2 Crystal structure of $Ca_{0.5}La_{0.5}Fe_{12-y}O_{19-\delta}$

As shown in Figure 4-8, 4-9 and 4-10, in order to investigate the influence of iron-deficiency on the composition and lattice parameter of Ca,La-M hexaferrite powders, X-ray diffraction patterns of calcined $Ca_{0.5}La_{0.5}Fe_{12-y}O_{19-\delta}$ powders at 1200, 1250 and 1300℃ for 12h in air were carried out. The results indicated that there was no single phase at 1200℃, and their iron solubility was restricted at a range of $1.75 \leqq y \leqq 2.15$ and $0.75 \leqq y \leqq 2.15$ at 1250 and 1300℃, respectively. After that, in order to investigate the magnetic properties, the calcined samples were sintered at 1275, 1300 and 1325℃ for 4 h in air, which were shown in Fig. 4-11 to 4-15.

Figu

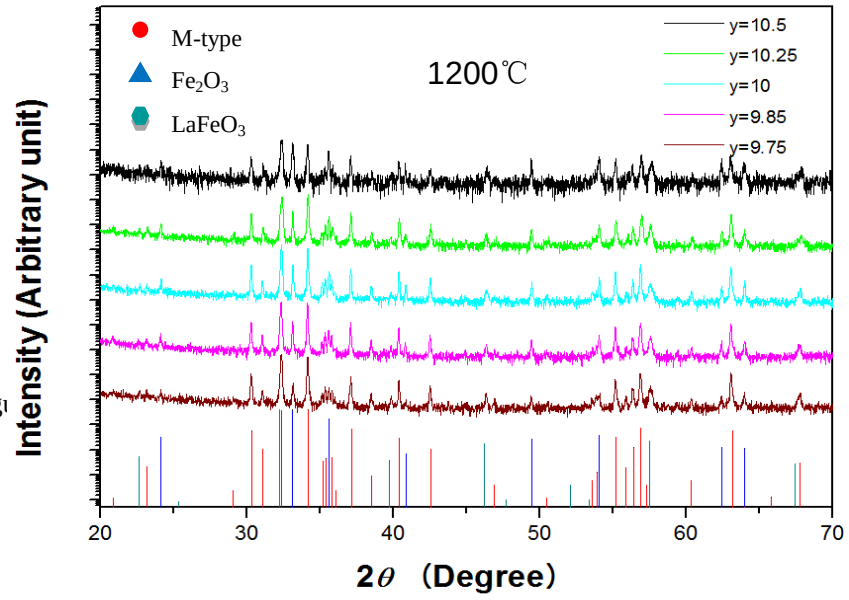

Figure 4-8 XRD patterns of $Ca_{0.5}La_{0.5}Fe_{12-y}O_{19-\delta}$ calcined in air.

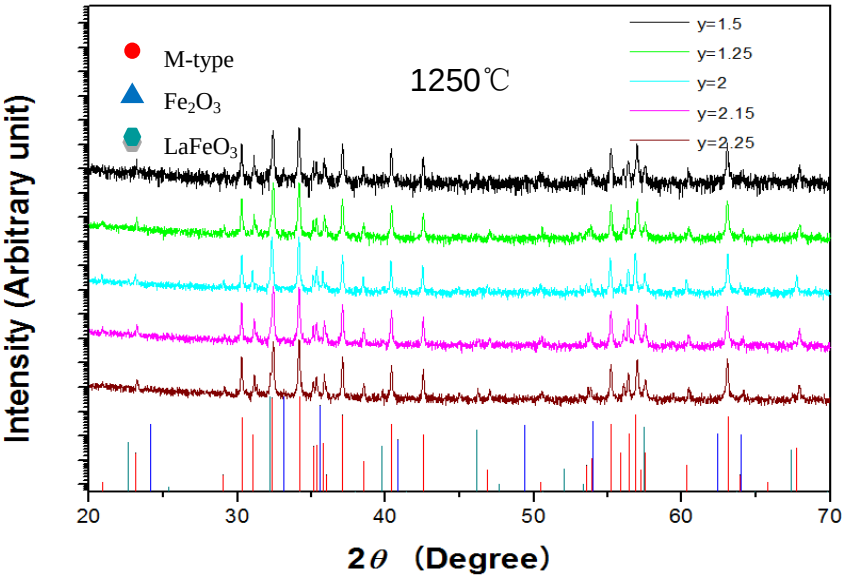

Figure 4-9 XRD patterns of $Ca_{0.5}La_{0.5}Fe_{12-y}O_{19-\delta}$ calcined in air

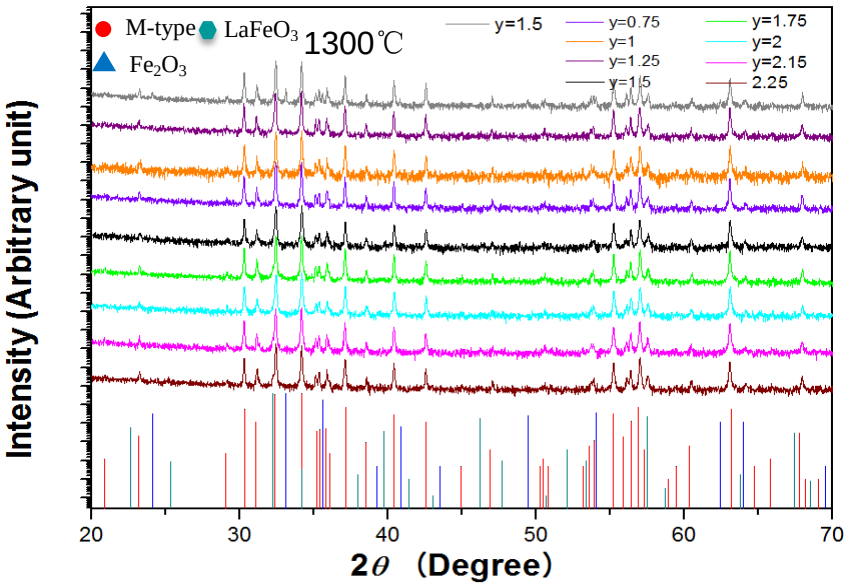

Figure 4-10 XRD patterns of $Ca_{0.5}La_{0.5}Fe_{12-y}O_{19-\delta}$ calcined in air

Table 4-4 Detected phases from XRD patterns of $Ca_{1-x}La_xFe_{12-y}O_{19-\delta}$ after calcination in air

Temperature (℃) / Composition.y	1200	1250	1300		1300
y=1.50	M+h+L	M+h	M		
y=1.75	M+h+L	M	M	y=0.5	M+h
y=2.00	M+h+L	M	M	y=0.75	M
y=2.15	M+h+L	M	M	y=1.0	M
y=2.25	M+h+L	M+L	M+L	y=1.25	M

M: M-type phase h: hematite L: $LaFeO_3$

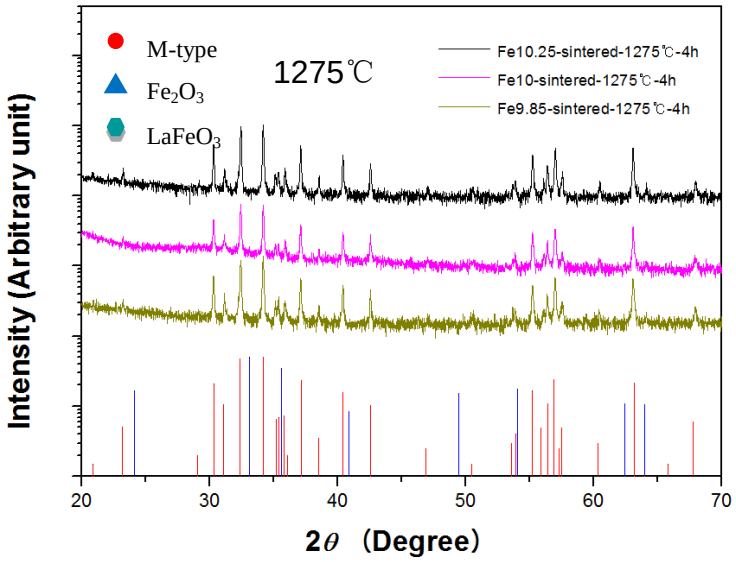

Figure 4-11 XRD patterns of $Ca_{0.5}La_{0.5}Fe_{12-y}O_{19-\delta}$ sintered in air.

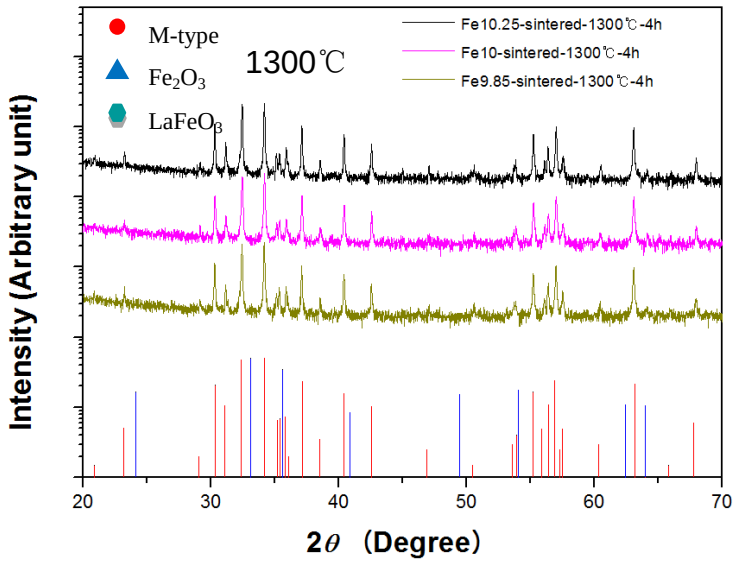

Figure 4-12 XRD patterns of $Ca_{0.5}La_{0.5}Fe_{12-y}O_{19-\delta}$ sintered in air.

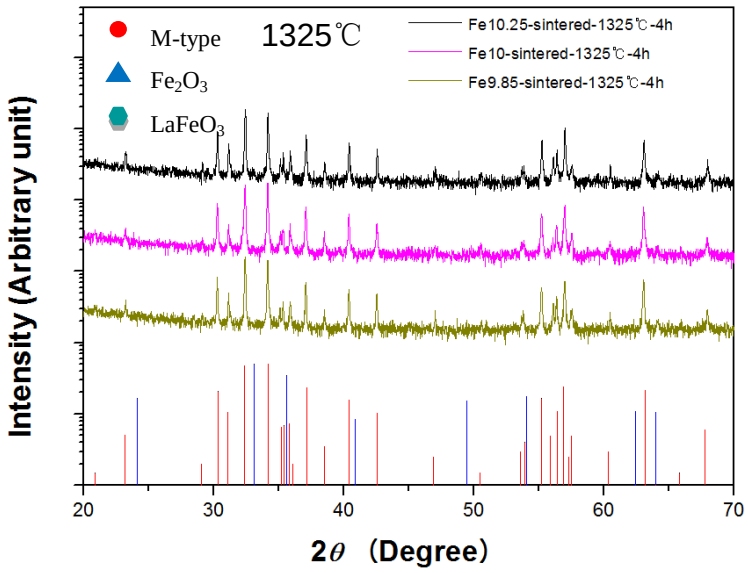

Figure 4-13 XRD patterns of $Ca_{0.5}La_{0.5}Fe_{12-y}O_{19-\delta}$ sintered in air

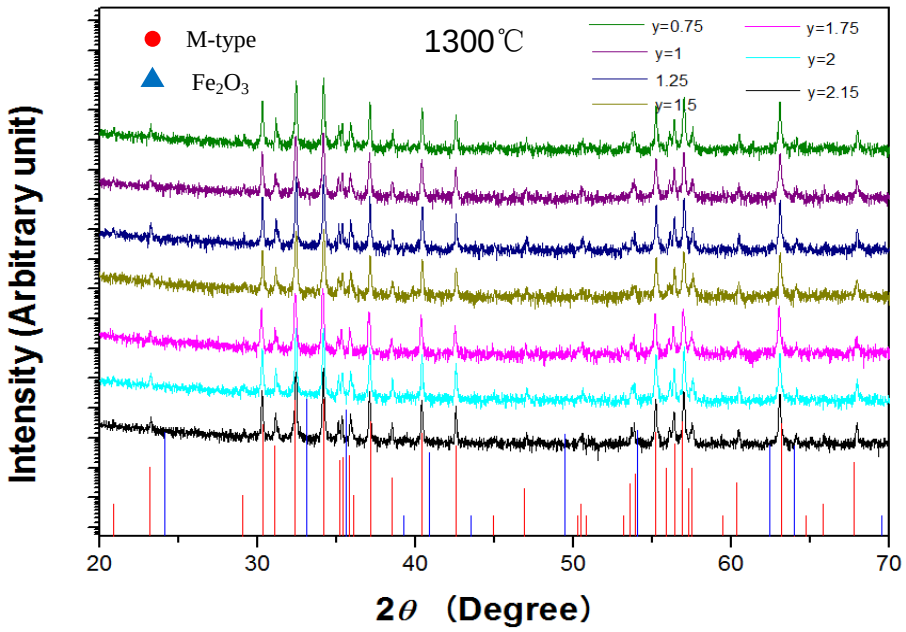

Figure 4-14 XRD patterns of $Ca_{0.5}La_{0.5}Fe_{12-y}O_{19-\delta}$ sintered in air

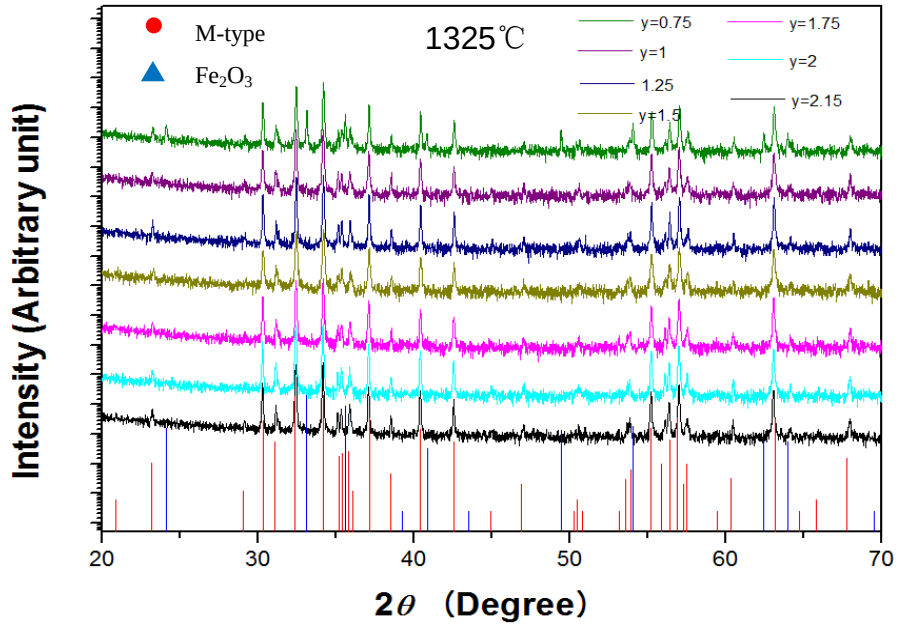

Figure 4-15 XRD patterns of $Ca_{0.5}La_{0.5}Fe_{12-y}O_{19-\delta}$ sintered in air

As shown in Figure 4-16, the samples were calcined at 1250℃ in air and as-calcined samples were sintered at 1275, 1300 and 1325℃. For the series of samples, the calculated lattice parameters *a*, *c*, and cell volume were listed in table 4-5, 4-6. Values for *a* and *c* were calculated from the values of d_{hkl} according to the following equation (4-1) [34]:

$$d_{hkl} = \left\{ \frac{4(h^2 + hk + k^2)}{3a^2} + \frac{l^2}{c^2} \right\}^{-1/2} \qquad (4\text{-}1)$$

Where d_{hkl} is the inner-planer spacing, and h, k and l are the Miller indices. The lattice parameters were shown in table as follows Fig 4-16, 4-17.

Both parameters a and c were firstly decreased as the content of Fe varying from 10.25 to 10 ($1.75 \leqq \boldsymbol{y} \leqq 2$), and due to a decline of the content of Fe^{3+} ions, the value of parameter c decreased with a slightly change in parameter a. From 10 to 9.85 ($2 \leqq y \leqq 2.15$), a possible reason for increasing of c and a was attributed to the content of O^{2-} increased, the radius of O^{2-} was larger than Fe^{3+} (O^{2-} = 0.138 nm，Fe^{3+} = 0.055 nm) [35]. Samples as shown in Fig. 4-17 were calcined at 1300℃ and as-calcined were sintered at 1300 and 1325℃, the trend of which was the same as that of Figure 4-16. In addition, cell volume was decreased initially and then increased substantially with the reduction of Fe content,

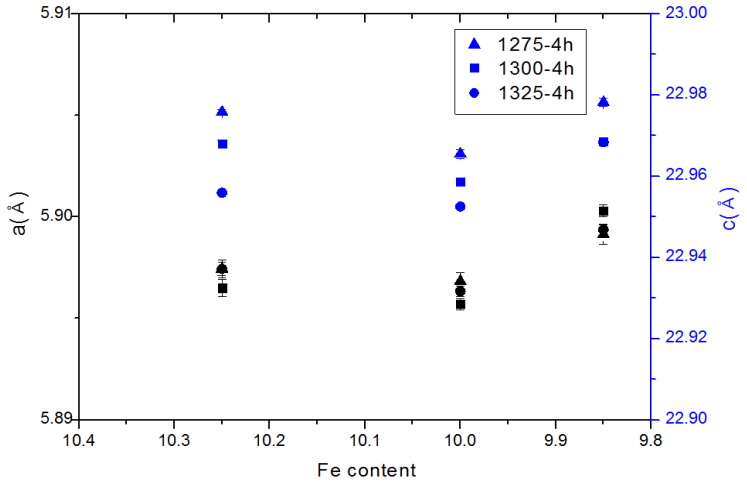

(a)

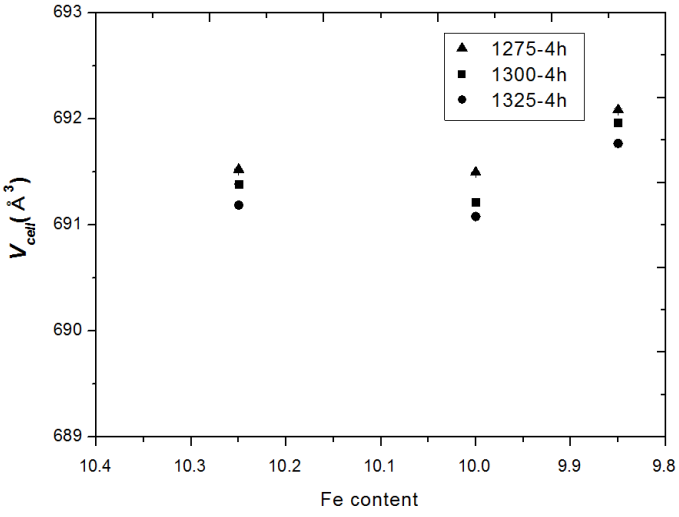

(b)

Figure4-16 Lattice parameters (a) and Cell volume (b) vs Fe content $Ca_{0.5}La_{0.5}Fe_{12-y}O_{19-\delta}$ calcined at 1250℃ for 12h in air.

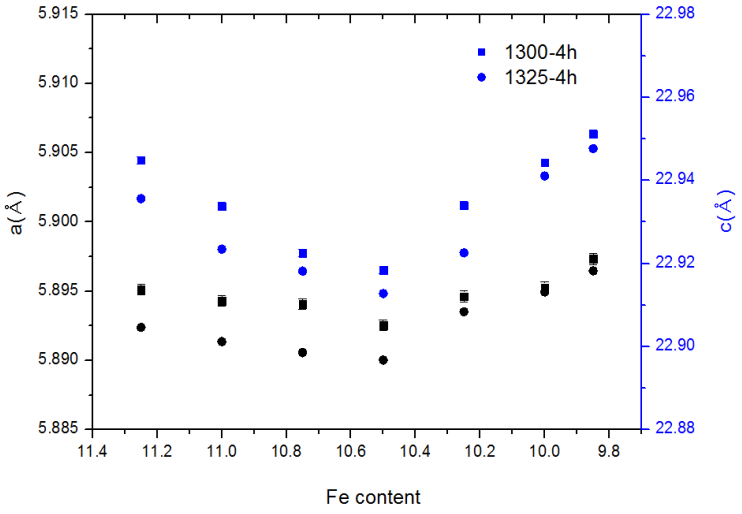

(a)

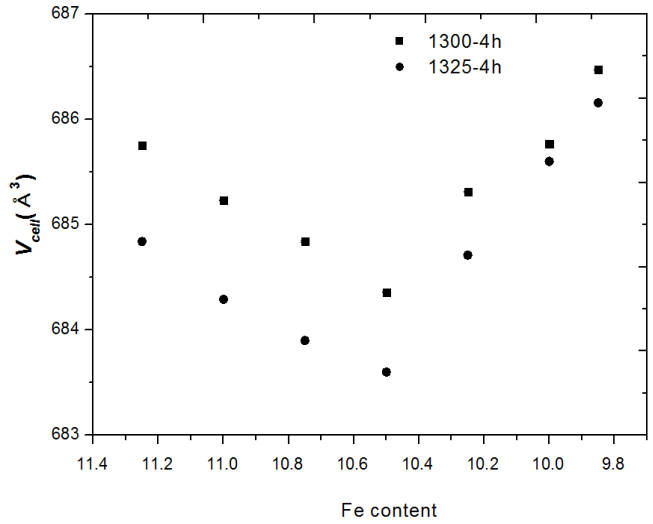

(b)

Figure 4-17 Lattice parameters (a) and Cell volume (b) vs Fe content $Ca_{0.5}La_{0.5}Fe_{12-y}O_{19-\delta}$ calcined at 1300℃ for 12h in air.

Table 4-5 Cell parameters and unit cell volumes are listed for $Ca_{0.5}La_{0.5}Fe_xO_{19-\delta}$ (Calcined 1250℃-12h in air)

Sintering temperature (℃)	Fe content x	a (Å)	c (Å)	Unit cell volume ($Å^3$)
1275	10.25	5.8973(2)	22.9758(9)	691.52(1)
	10.00	5.8968(3)	22.9655(10)	691.49(1)
	9.85	5.8991(2)	22.9782(10)	692.08(2)
1300	10.25	5.8965(3)	22.9680(10)	691.39(2)
	10.00	5.8957(2)	22.9586(9)	691.22(1)
	9.85	5.9003(3)	22.9685(10)	691.96(2)
1325	10.25	5.8975(3)	22.9558(9)	691.19(2)
	10.00	5.8963(3)	22.9525(10)	691.06(2)
	9.85	5.8993(2)	22.9683(9)	691.75(1)

Table 4-6 Cell parameters and unit cell volumes are listed for $Ca_{0.5}La_{0.5}Fe_xO_{19-\delta}$ (Calcined 1300℃-12h in air)

Sintering temperature (℃)	Fe content x	a (Å)	c (Å)	Unit cell volume ($Å^3$)
1300	11.25	5.8951(3)	22.9448(10)	685.75(2)
	11.00	5.8943(3)	22.9337(11)	685.23(2)
	10.75	5.8941(2)	22.9225(9)	684.84(1)
	10.50	5.8925(3)	22.9184(10)	684.36(2)
	10.25	5.8946(2)	22.9339(10)	685.31(2)
	10.00	5.8953(2)	22.9443(9)	685.77(1)
	9.85	5.8973(2)	22.9512(10)	686.37(2)
1325	11.25	5.8924(3)	22.9356(11)	684.84(2)
	11.00	5.8913(2)	22.9234(10)	684.29(2)
	10.75	5.8906(3)	22.9182(10)	683.92(2)
	10.50	5.8901(3)	22.9127(9)	683.58(1)
	10.25	5.8935(3)	22.9226(9)	684.71(1)
	10.00	5.8949(2)	22.9411(10)	685.62(2)
	9.85	5.8965(2)	22.9476(10)	686.16(1)

4.3 Microstructure and morphology of $Ca_{0.5}La_{0.5}Fe_{12-y}O_{19-\delta}$.

SEM micrographs of samples with different Fe content(x) of 11.25, 11.00, 10.75, 10.50, 10.25, 10.00, and 10.75 were shown in Fig. 4-18. As shown in this figure, it is observed that the hexaferrite magnets are formed of hexagonal-shaped crystals, and the phases were perfect crystalline hexaferrite. The average grain sizes were measured from the SEM micrographs using an image-analyzing program (Image-Pro Plus). The average grain size was about 10 μm, which initially increased but later reduced with y increasing. The grain size distribution was shown in Fig. 4-19.

As Fe content decreased, iron vacancy and oxygen vacancy of crystal structure existed were increased, which could induce to an increase of grain size.

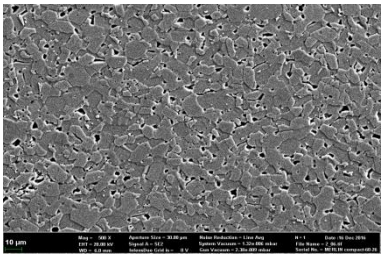

x=11.25

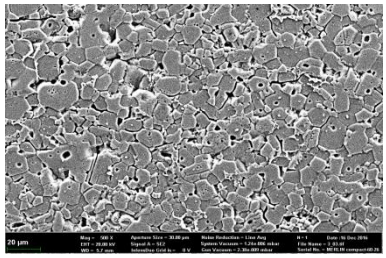

x=11.00

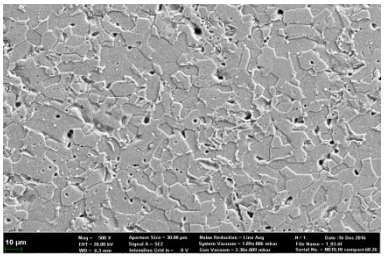

x=10.75

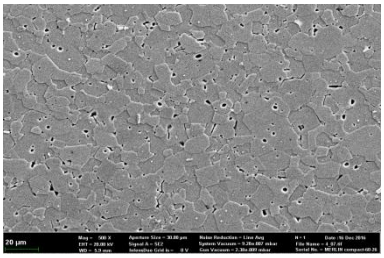

x=10.50

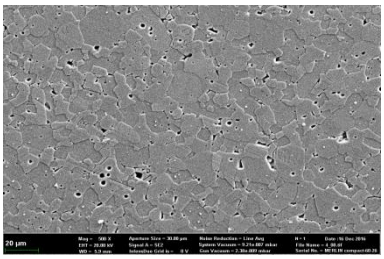

x=10.25

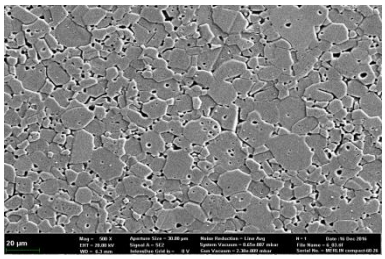

x=10.00

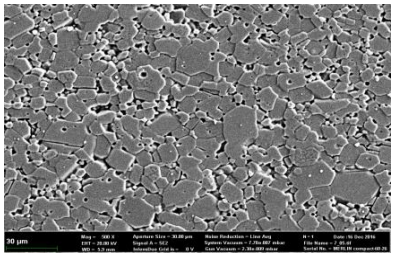

x=9.85

Figure 4-18 SEM images of $Ca_{0.5}La_{0.5}Fe_{12-y}O_{19-\delta}$ Compositions sintered at 1300℃ for 4h in air after calcination at 1300℃ for 12h in air.

Table 4-7 Grain size distribution of $Ca_{0.5}La_{0.5}Fe_{12-y}O_{19-\delta}$ compositions sintered at 1300℃ for 4h after calcination at 1300℃ for 12h in air

Fe content (y)	Ave. Grain Size(μ m)
0.75	9.5
1.00	9.6
1.25	9.7
1.50	10.2
1.75	9.8
2.00	9.7
2.15	9.5

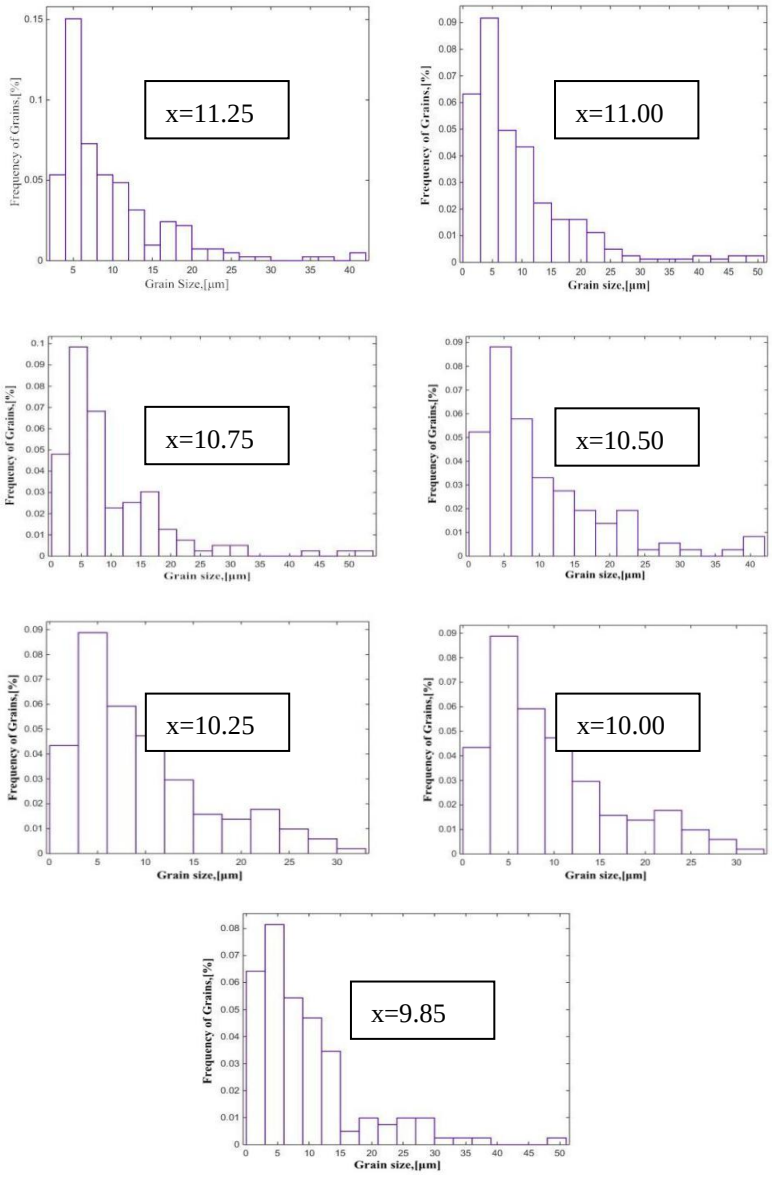

Figure 4-19 Grain size distribution of $Ca_{0.5}La_{0.5}Fe_{12-y}O_{19-\delta}$ composition sintered at 1300℃ for 4h in air after calcination at 1300℃ for 12h in air.

4.4 Magnetic properties of $Ca_{0.5}La_{0.5}Fe_{12-y}O_{19-\delta}$

Hysteresis loops of $Ca_{0.5}La_{0.5}Fe_{12-y}O_{19-\delta}$ are shown in Fig. 4-20, 4-21, 4-22, 4-23, and 4-24. The magnetization datum fitted by applying the law of approach to saturation, as denoted by equation (4-2) [36, 37].

$$M = M_S(1 - A/H - B/H^2) + \chi_P H \qquad (4\text{-}2)$$

In which M_s is the saturation magnetization. The term represents the field-induced increase in the spontaneous magnetization of the domains, or forced magnetization; this term is usually small at temperatures well below the Curie point and may often be neglected. Constant A is generally interpreted as due to inclusions and microstress, and constant B is proportional to K^2 (K is the anisotropy constant). And at high magnetic field, the term *A/H* could be neglected too. Thus the equation (4-2) can be expressed as (4-3) [38].

$$M = M_S(1 - B/H^2) \qquad (4\text{-}3)$$

Therefore at high applied magnetic field, M-H curves are fitted by equation (4-3).We can evaluate the values of M_s.

From the hysteresis loops, to the H_c and M_r values, correspondingly, we can get positive value and negative value. And get the average value between them. It is the H_c and M_r values. From the table 4-7, 4-8, note that M_s is decreased with y increasing, but not significantly. M_s *is slightly* modified in all samples since its value depend on composition, crystallinity and the presence of

non-magnetic phases as hematite. Due to the non-magnetic phase hematite, the lower saturation magnetization value of 58.9 emu/g was obtained for the $Ca_{0.5}La_{0.5}Fe_{12-y}O_{19-\delta}$ ($0.75 \leqq y \leqq 2.15$) sample which was calcined at 1300℃-12 h in air prepared at y is 0.75 and sintered at 1325℃-4 h in air; The maximum M_s was 77.5 emu/g at 1300℃-4 h in air, when y is 0.75. As y increases, H_c first decrease and then increase for all Fe composition(y). Because the amount of Fe^{3+} decreased, it makes the Fe-O-Fe super exchange interaction proportionally weak, resulting in decreased M_s.

There is a close relation between H_c and grain size. Based on the previous SEM investigations, it has been shown that an increase is observed before the decline in grain size. Thus, H_c shows a decrease before an increase in grain size [Table 4.7].

As reported in the research[39]，the authors suggested that a lower Fe^{3+}/Sr^{2+}mole ratio than stoichiometry leads to the production of iron and oxygen vacancies，a phenomenon which is similar to the present experiment where the lower Fe^{3+}/Ca^{2+} or La^{3+} enhances the ionic diffusion and improve the magnetic properties. However, the images taken by SEM showed the average grain size is larger than the size of single domain; it could result in the small value of H_c.

Though the comparison table 4-9, we can see the value of M_s of Sr-Ca-La-Co M-type hexaferrite is larger than that of the pure Sr or Ba M-type hexaferrite

without substitution. And for the Ba-Ir-Co-Bi M type hexaferrite, due to the substitution of Ir and Bi, the higher M_s=86 emu/g was obtained. In my study, the M_s = 77.5 emu/g of composition $Ca_{0.5}La_{0.5}Fe_{11.25}O_{19-\delta}$ without Sr and Co substitution, but less content of Fe than stoichiometry, was obtained.

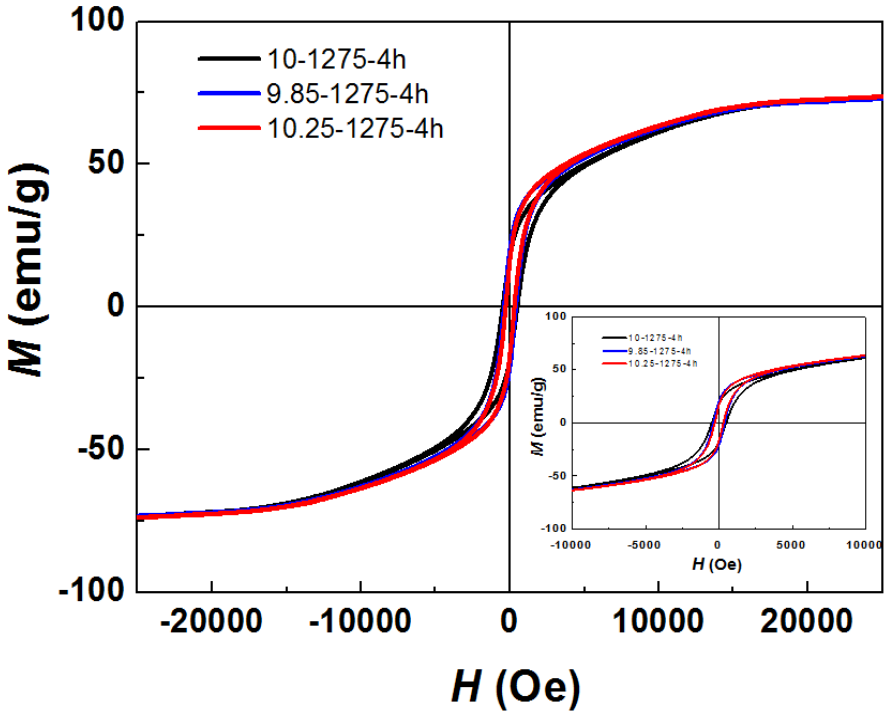

Figure 4-20 Hysteresis loops for $Ca_{0.5}La_{0.5}Fe_{12-y}O_{19-\delta}$ (1.75 ≦ y ≦2 .15) sintered at 1275℃ for 4h in air.

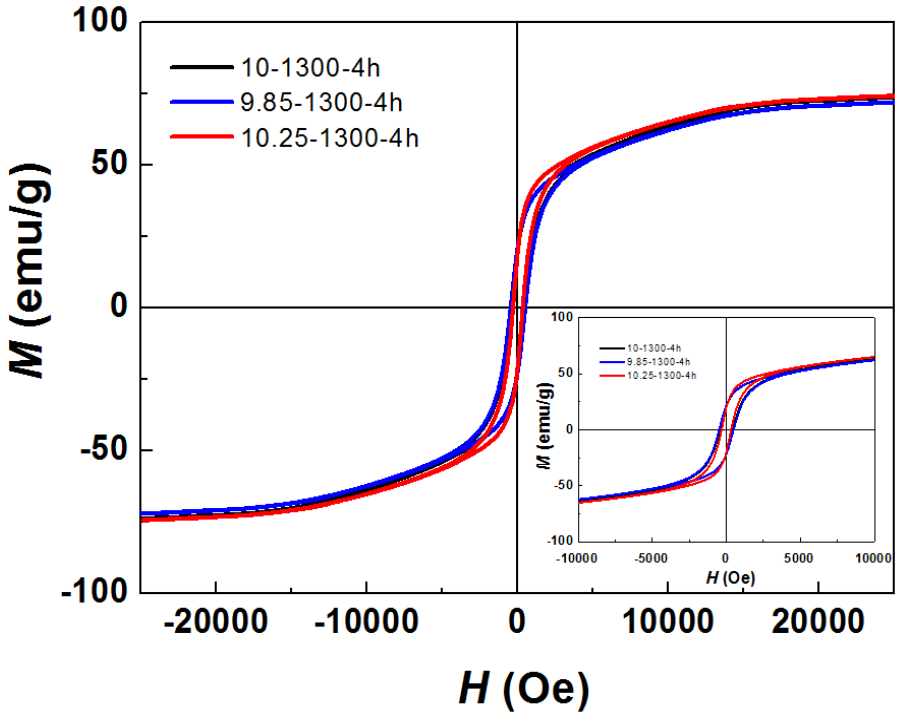

Figure 4-21 Hysteresis loops for $Ca_{0.5}La_{0.5}Fe_{12-y}O_{19-\delta}$ (1.75 ≦ y ≦ 2.15) sintered at 1300℃ for 4h in air.

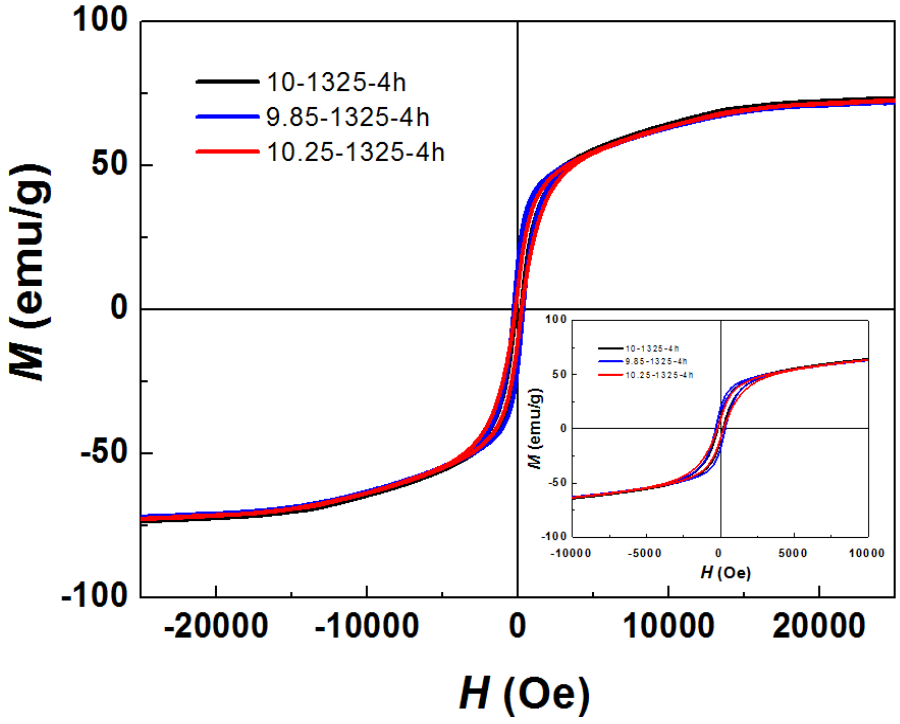

Figure 4-22 Hysteresis loops for $Ca_{0.5}La_{0.5}Fe_{12-y}O_{19-\delta}$ (1.75 ≦ y ≦ 2.15) sintered at 1325℃ for 4h in air.

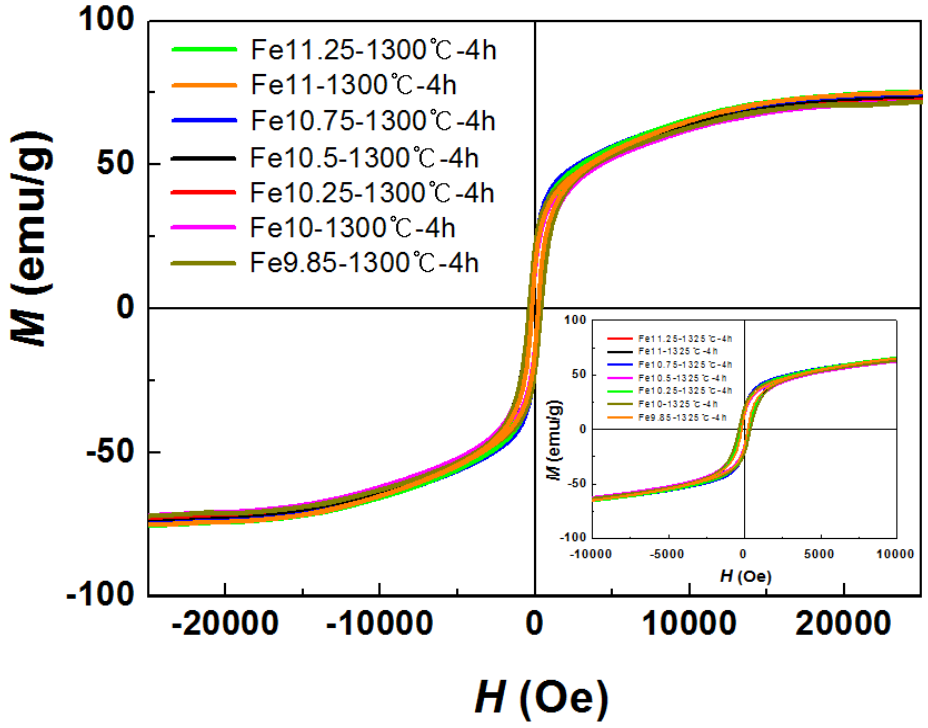

Figure 4-23 Hysteresis loops for $Ca_{0.5}La_{0.5}Fe_{12-y}O_{19-\delta}$ (0.75 ≦ y ≦ 2.15) sintered at 1300℃ for 4h in air.

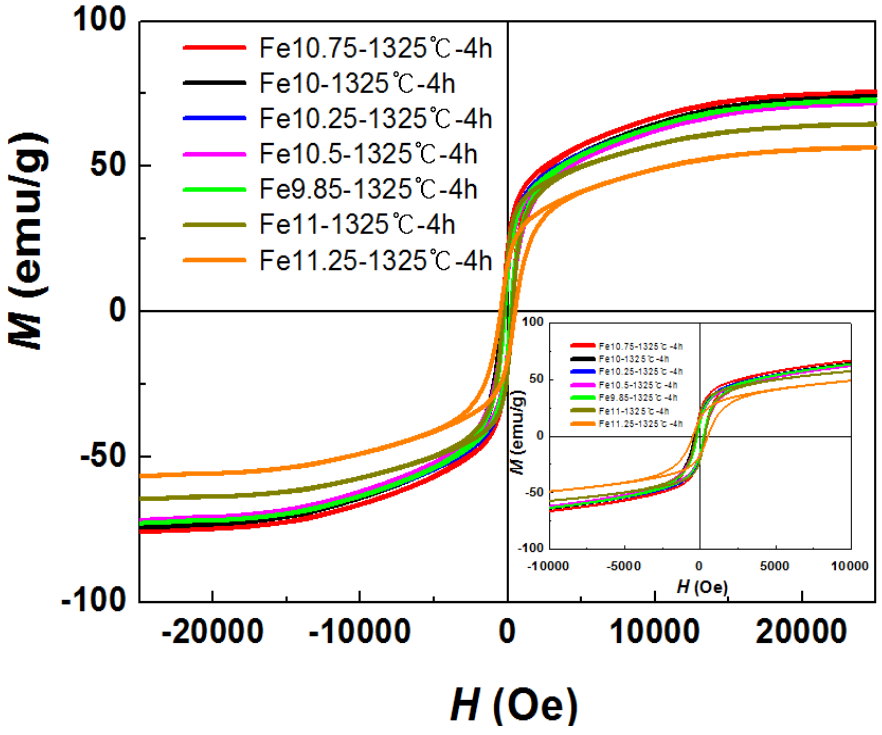

Figure4-24 Hysteresis loops for $Ca_{0.5}La_{0.5}Fe_{12-y}O_{19-\delta}$ (0.75 ≦ y ≦2.15) sintered at 1325℃ for 4h in air.

Table 4-8 Magnetic properties of $Ca_{0.5}La_{0.5}Fe_{12-y}O_{19-\delta}$ ($1.75 \leqq y \leqq 2.15$) sintered in air

Sintering temperature (℃)	Fe content (y)	M_s (emu/g)	M_r (emu/g)	H_c (Oe)
1275	1.75	75.9	16.6	393
	2.00	75.6	20.5	294
	2.15	74.7	18.1	483
1300	1.75	75.6	21.1	440
	2.00	75.5	20.0	325
	2.15	74.5	21.7	484
1325	1.75	74.9	10.1	211
	2.00	74.2	8.9	187
	2.15	73.8	18.4	317

Table 4-9 Magnetic properties of $Ca_{0.5}La_{0.5}Fe_{12-y}O_{19-\delta}$ ($0.75 \leqq y \leqq 2.15$) sintered in air

Sintering temperature (℃)	Fe content (y)	M_s (emu/g)	M_r (emu/g)	H_c (Oe)
1300	0.75	77.5	18.7	296
	1.00	77.3	18.6	290
	1.25	77.3	17.3	270
	1.50	77.1	14.1	216
	1.75	76.9	15.7	258
	2.00	76.0	19.3	323
	2.15	74.5	21.3	387
1325	0.75	58.9	16.3	492
	1.00	66.2	19.8	304
	1.25	77.2	16.2	291
	1.50	76.2	13.4	211
	1.75	74.8	23.4	246
	2.00	74.1	16.6	260
	2.15	73.8	18.8	305

Table 4-10 Comparison of saturation magnetization of M-type hexaferrites

Composition	M_s (emu/g)	Reference
$SrFe_{12}O_{19}$	Up to 70	[40]
$BaFe_{12}O_{19}$	68	[41]
$Sr_{0.65-x}Ca_xLa_{0.35}Fe_{11.32}Co_{0.28}O_{18.435}$	75.3(x=0.2)	[42]
$BaFe_{10.25}Ir_{0.85}Co_{0.85}Bi_{0.05}O_{19}$	86	[43]
$Ca_{0.5}La_{0.5}Fe_{10.25}O_{19-\delta}$	75.9	Present study
$Ca_{0.5}La_{0.5}Fe_{11.25}O_{19-\delta}$	77.5	Present study

Table 4-11 Density and relative density of $Ca_{0.5}La_{0.5}Fe_{12-y}O_{19-\delta}$ ($1.75 \leqq y \leqq 2.15$) sintered in air

Sintering temperature(℃)	Fe content (y)	Density (g/cm^3)	Relative density (%)
1325	1.75	4.84(2)	91.6
	2.00	4.95(3)	93.7
	2.15	4.72(6)	91.3
1300	1.75	4.76(3)	91.1
	2.00	4.93(3)	93.3
	2.15	4.68(5)	90.9
1275	1.75	4.72(2)	90.9
	2.00	4.89(4)	92.6
	2.15	4.61(4)	90.2

Table 4-12 Density and relative density of $Ca_{0.5}La_{0.5}Fe_{12-y}O_{19-\delta}$ ($0.75 \leqq y \leqq 2.15$) sintered in air

Sintering temperature(℃)	Fe content (y)	Density (g/cm^3)	Relative density (%)
1325	0.75	4.76(5)	91.3
	1.00	4.82(3)	91.6
	1.25	4.86(4)	92.6
	1.50	4.98(5)	92.4
	1.75	4.77(3)	91.1
	2.00	4.68(6)	90.5
	2.15	4.63(3)	90.3
1300	0.75	4.65(6)	90.5
	1.00	4.78(6)	91.2
	1.25	4.84(4)	92.5
	1.50	4.92(5)	92.2
	1.75	4.69(3)	90.7
	2.00	4.61(5)	90.1
	2.15	4.65(6)	90.5

5. Conclusion

In this study, $Ca_{1-x}La_xFe_{12}O_{19}$ and $Ca_{0.5}La_{0.5}Fe_{12-y}O_{19-\delta}$ were prepared by conventional solid state reaction. The effect of iron deficiency on crystal structure and magnetic properties of $Ca_{0.5}La_{0.5}Fe_{12-y}O_{19-\delta}$ were systematically investigated.

The compound $Ca_{0.5}La_{0.5}Fe_{12-y}O_{19-\delta}$ was synthesized by calcication at 1250 and 1300℃ for 12h in air, and its iron solubility limits were $1.75 \leqq \boldsymbol{y} \leqq 2.15$ and $0.75 \leqq \boldsymbol{y} \leqq 2.15$, respectively. Thereby, we concluded that iron deficiency could be a beneficial factor for synthesis of single phase Ca-La M-type hexagonal ferrite.

In addition, for the single phase $Ca_{0.5}La_{0.5}Fe_{12-y}O_{19-\delta}$ ferrite, at a given sintering temperature, 1275, 1300, and 1325℃ for 4 h in air, the lattice parameters *a*, *c* and the unit cell volume were all decreased initially but increased later with increasing y. It was revealed from SEM investigations that the average grain size of the sample with the same sintering condition was about 10 μm and it shows a opposite tendency, initial increase followed by an decrease with respect to y sintered at 1300℃ for 4h. Also, as y increased, the saturation magnetization M_s continued to slightly decrease. And H_c initially decreased but increased later. Iron deficiency can lead to the production of

iron and oxygen vacancies, which could enhance the diffusion among various ions. Thus the magnetic properties could be improved, and the highest M_s of 77.5 emu/g was obtained at y = 0.75 for the sample sintered at 1300℃ for 4h in air, which was higher than those of pure phase Sr-hexaferrite (SrM) and Ba-hexaferrite (BaM) by 11.2% and 14.5%, respectively.

References

[1] S.V. Ketov, Yu.D. Yagodkin, V.P. Menushenkov, Journal of Alloys and Compounds, 509, 1065–1068 (2011)

[2] N. Chen, K. Yang, M. Gu, Journal of Alloys and Compounds, 490, 609–612 (2010)

[3] Liu X S, Zhong W, Gu B X et al, Rare Metal Materials and Engineering, 31-5: 385 (2002)

[4] Dai Q, Berman D, Virwani K et al. Nano Letters. 10, 3216-3221(2010)

[5] C. Sudakar, G.N. Subbanna, T.R.N. Kutty, Journal of Magnetism and Magnetic Materials, 263, 253-268 (2003)

[6] M. Zheng and X. Y. Li and M. M. Yang and Q. X. Zhu and Y. Wang and X. M. Li and X. Shi and H. L. W. Chan and X. G. Li and H. S. Luo and R. K. Zheng, Applied Physics Letters,103,253-506(2013)

[7] Liu X S, Hernández-Gómez P, Huang K et al. Journal of Magnetism and Magnetic Materials, 112, 305-341(2006)

[8] Pang Z, Zhang X, Ding B et al, Journal of Alloys and Compounds, 492, 653-691(2010)

[9] Liu X S, Zhong W, Yang S et al. Journal of Magnetism and Magnetic Materials, 238, 207-235(2002)

[10] Liu X S, Hernández-Gómez P, Deng X Y et al. Journal of Magnetism and Magnetic Materials, 321, 242-286(2009)

[11] Rezlescu N, Doroftei C, Rezlescu E et al. Journal of Alloys and Compounds, 451,98-121(2008)

[12] Mozaffari M, Arab A, Yousefi M H et al. Journal of Magnetism and Magnetic Materials, 326, 32-56(2010)

[13] Gama L, Diniz A P, Costa A C F M et al. Physica B, 384, 97-99(2006)

[14] Zhang Y, Wen D, Advanced Materials, 311, 217-218(2011)

[15] Seifert D, Töpfer J, Langenhorst F et al, Journal of Magnetism and Magnetic Materials, 321, 4045-4051(2009)

[16] P. B. Braun, Philips Research Report, 12, 491-495 (1957)

[17] B. Phillips, A. Muan, Journal of the American Ceramic Society, 41, 445–454 (1958).

[18] N. Ichinose, K. Kurihana, Japan of Physical Society, 18, 1700-1701 (1963).

[19] H.Yamamoto, T. Kawaguchi, and M. Nagakura, Journal of the Japan Society of Powder and Powder Metallurgy, 25, 242-248（1978）

[20] H. Yamamoto, T. Kawaguchi, M. Nagakura, and Y. Kohayashi, Journal of the Japan Society of Powder and Powder Metallurgy, 25, 236-241(1978)

[21] H. Yamamoto, T. Kawaguchi, M. Nagakura, IEEE Transactions on Magnetics, 15, 1141-1146 (1979).

[22] J. Bai, X.S Liu, T. Xie, F. Wei, Z. Yang, Materials Science and Engineering , 68, 182-185(2000)

[23] Q.Q. Fang, W. Zhong, Y.W. Du, Chinese Physics Letters, 16, 285-287(1999)

[24] Y.K. Liu, Y.J. Feng, X.W. Wu, Y. Wang, L. Cai, Y.X.Ke, Y.Gong, Material

Science and Technology, 18, 262-266(2010)

[25] P.E. Kazin, L.A. Trusov, D.D. Zaitsev, Y.D. Tret'Yakov, Russian Journal of Inorganic Chemistry, 54, 2081-2090(2009)

[26] R. Müller, R. Hiergeist, W. Gawalek, A. Hoell, A. Wiedenmann, Journal of Magnetism and Magnetic Materials, 252, 43-45(2002)

[27] R. Murakami, K. Shima, H. Kakuta, H. Takamura, T. Tanaka, M. Okada, M.Fukuda, M. Sano, K. Kamino, Materials Transactions, 37, 499-502(1996)

[28] Z.W.Li, L.Chen, C.K.Ong, Journal of Applied Physics, 923902-3907(2002)

[29] T. Zemcik, Fresenius I, Journal of Analytical Chemistry, 349 26-31(1994)

[30] G Albanese, A. Deriu, G Calestani, R Leccabue, B.E. Watts, Journal of Materials Science, 27, 6146-6150(1992)

[31] H. Yamamoto, F. Oyobi F. Yakin, Journal of the Japan Society of Powder and Powder Metallurgy, 43, 5-12(1996)

[32] H. Sato, T. Umeda, Y. Kimura, Nippon Kinzoku Gakkaishi. Journal of the Japan Society of Powder and Powder Metallurgy, 45(2000)6-13

[33] Q.Q. Fang, W. Zhong, Y.W. Du, Chinese Physics Letters, 16, 285-287(1999)

[34] Y.M Kang, Y.H Kwon, M.H Kim, D.Y Lee, Journal of Magnetism and Magnetic Materials, 382, 10-14(2015)

[35] T.T Fang, K.T Lee, Journal of the American Ceramic Society,72, 2034-2039(1989)

[36] A. Kihal, G. Fillion, B. Bouzabata, B. Barbara, Physica Status Solidi, 249, 604-614(2012)

[37] S. Ounnunkad, P. Winotai, Journal of Magnetism and Magnetic Materials, 301, 292–300(2006)

[38] B.G. Toksha, Solid State Communications, 147, 479–483(2008)

[39] F.L Zan, Y.Q Ma, X Zhang, Q Ma, G.H Zheng, Z.X Dai, Journal of Anhui University, 38, 45-54(2014)

[40] H.S özeri, A.Baykal, B. Ünal, physica status solidi, 209, 2002-2013 (2012)

[41] Kojima H, Ferromagnetic materials, 3, 658-659 (1982)

[42] Y.J Yang, X.S Liu, Transactions on magnetics, 50, 234-236(2013)

[43] B. Sugg, H. Vincent, Journal of Magnetism and Magnetic Materials, 139, 364-370(1995)

초록

Ca-La M-type 헥사페라이트는 Sr 이나 Ba 같은 M-type 에 비교하면 높은 포화 자화(Ms) 그리고 항자기성(Hc)을 가지고 있습니다. 본 연구에서는 $Ca_{1-x}La_xFe_{12}O_{19}$ 를 성공적으로 합성하였고 철 함량에 따른 $Ca_{0.5}La_{0.5}Fe_{12-y}O_{19-\delta}$ ($0.75 \leqq y \leqq 2.15$) M-type 헥사페라이트 구조적인 영향과 자기적성질에 대해서 탐구 하였습니다.

Ca-La M-type 헥사페라이트 파우더는 $Ca_{1-x}La_xFe_{12}O_{19}$ (x=0.4, 0.5 and 0.6) 그리고 $Ca_{0.5}La_{0.5}Fe_{12-y}O_{19-\delta}$ ($0.75 \leqq y \leqq 2.15$)는 기본적인 고체상태로 반응을 시켰고 사용된 파우더는 순도 (La_2O_3, $CaCO_3$, Fe_2O_3)가 99.9%인 고체로 사용하였습니다. 우선 파우더를 사용할 만큼 무게를 재고, 24 시간 ball-milling 시킨뒤, 펠렛에 누른 상태로 고정 시킵니다. 다음 펠렛을 차례로 1150, 1200, 1250, 그리고 1300℃ 로 12h 하소시키고 싱글상태인 M-type 헥사페라이트가 형성이 되는지 확인합니다. 하소를 ball milling 그리고 펠렛 만드는 과정에도 절차를 반복하였습니다. 하소가 끝난 파우더는 펠렛에 단축으로 깔아놓고, 샘플 자체 자기적 물성을 보기 위하여 펠렛을 퍼니스에 넣고 공기가 있는 상태에서 1275, 1300 그리고 1325℃ 온도를 주고 4h

신터링 시켜줍니다. 샘플 물리적 상태 그리고 결정구조와 같은 파라메터들은 X-ray diffraction (XRD)를 통하여 확인하였습니다. 마이크로구조는 Field Emission-scanning electron microscopy (FE-SEM) 을 사용하여 측정 하였고 자기적 성질은 Vibrating Sample Magnetometer (VSM)으로 확인 하였습니다.

XRD 패턴으로 1250℃ 에서 12h 하소한 $Ca_{0.5}La_{0.5}Fe_{12-y}O_{19-\delta}$ ($1.75 \leqq y \leqq 2.15$) 샘플과 1300℃ 에서 12h 하소한 $Ca_{0.5}La_{0.5}Fe_{12-y}O_{19-\delta}$ ($0.75 \leqq y \leqq 2.15$) 샘플이 hexagonal 결정구조인것을 확인할 수 있었고 싱글 구조인 $Ca_{0.5}La_{0.5}Fe_{12-y}O_{19-\delta}$ 샘플은 라텍스 파라메터 *a*, *c* 그리고 unit cell 볼륨이 신터링 과정을 통하여 y 가 증가함에 따라 감소하다가 다시 증가되는 것을 알 수 있습니다. 평균 입자 사이즈도 y 가 증가함에 따라 처음에 감소하다가 다시 증가되는 것을 확인할 수 있습니다. 포화 자화 상수(M_s)는 y 가 증가함에 따라 감소되는 것을 알 수 있었고 최대치는 77.5 emu/g 로 $Ca_{0.5}La_{0.5}Fe_{12-y}O_{19-\delta}$ (y=0.75) 샘플이 1300℃ 에서 4h 신터링 시켜 얻은 결과임을 확인할 수 있었습니다. 실험 결과로 제조한 샘플 또한 SrM (11.2%) 그리고 BaM(14.5%) 보다 높다는 것도 알 수 있습니다. y 값이 증가함에 따라 H_c 도 첨에 감소하다가 다시 증가되는 것을 확인 하였습니다.

실험결과로 정리하면, 철 함량에 따라서 싱글 구조인 Ca-La M-type

헥사페라이트를 제조 하였고, 화합물 $Ca_{0.5}La_{0.5}Fe_{12-y}O_{19-\delta}$ 은 1250 그리고 1300℃ 조건에서 12h 하소 시키고 철의 용해도는 $1.75 \leqq y \leqq 2.15$ 그리고 $0.7 \leqq y \leqq 2.15$ 범위에 있음을 검증 하였습니다. 철 함량은 Ca-La M-type 헥사페라이트 자기적 성질을 증가시킬 수 있음을 최종적으로 확인 하였습니다.

주요어: magnetoplumbite, 철이 부족, hexaferrite, Ca-La M-type hexaferrite, 고체상반응, 포화자화강도, 항자기력

학번: 2014-25146